Journal of Applied Mechanics and Technical Physics, Vol. 50, No. 4, pp. 684–690, 2009

ONE MODEL OF FATIGUE CRACK GROWTH

A. P. Shabanov

UDC 620.178.6

A model for crack growth is proposed based on studies of the variation in the curvature radius at the crack tip during cyclic loading. Relations are obtained between mechanical material characteristics, crack geometry, and the rate of crack growth in a structure under cyclic loading.

Key words: *fatigue crack, plastic zone, Paris law.*

1. Initial Propositions. The model of a fatigue crack is constructed using the following propositions.

1. A homogeneous and isotropic plastic material is considered whose idealized tension diagram can be represented as a Prandtl diagram with the following parameters: σ_y is the yield point of the material, ε_y is the strain corresponding to the yield point, $\varepsilon_{\lim}$ is the limiting strain, and E is the longitudinal elastic modulus.

2. The sample is in a plane stress state.

3. The sample material is cyclically stable. During cyclic loading, the yield points in compression and tension and the limiting strain $\varepsilon_{\lim}$ do not change.

4. The dimensions of the plastic regions adjoining the crack tips are much smaller than the dimensions of the elastic regions of the sample.

5. The rigidity of the material is much more higher in the elastic region of the material sample than in the plastic region directly adjoining the crack tip. Therefore, it is assumed that the deformation of the plastic region from the side of the elastic region of the material is performed under rigid loading.

6. At infinity, the sample is subjected to stresses perpendicular to the direction of the crack. In the loading cycle, the maximum stresses are equal to $\sigma_{\max}$, and the minimum stresses $\sigma_{\min}$. The absolute value of the external stress does not exceed the yield point of the material.

7. In each external loading half-cycle, the cyclic loading of the sample is modeled by sequential application of tensile (during loading) and compressive (during unloading) stresses at infinity equal to $\sigma_{\max} - \sigma_{\min}$. We study the variation in the stress–strain state of the region adjoining the crack tip during loading from the value $\sigma_{\min}$ to the value $\sigma_{\max}$ and during unloading from the value $\sigma_{\max}$ to the value $\sigma_{\min}$.

8. Fracture of the material occurs at the time when the strains exceeds the limiting value $\varepsilon_{\lim}$. During compression, the strain is not limited.

9. The steady-state fracture process is analyzed. The crack geometry and the stress–strain state of the material at the crack tip have been formed as a result of the previous long cyclic loading of the sample. The crack start and fragile rupture mechanisms are not considered.

2. Elastoplastic Deformation of Crack-Like Defects. Let a sample have a crack-like defect of length $2l$ with tip curvature radius ρ. We establish the relationship between the external stress and plastic strain at the crack tip. For this, we write the Neuber relation for the concentration factors [1]

$$k_e^2 = k_\sigma k_\varepsilon, \tag{1}$$

where $k_e = \sigma_e/\sigma_n$, $k_\sigma = \sigma/\sigma_n = \sigma_y/\sigma_n$, $k_\varepsilon = \varepsilon/\varepsilon_n$, σ and ε are the stress and strain at the crack tip, σ_n and ε_n are the nominal stress and strain in the unperturbed region of the sample, related by the equality $\sigma_n = E\varepsilon_n$, and σ_e is

Siberian State University of Means of Communication, Novosibirsk 630049; shabanov@211.ru. Translated from Prikladnaya Mekhanika i Tekhnicheskaya Fizika, Vol. 50, No. 4, pp. 167–175, July–August, 2009. Original article submitted February 1, 2008; revision submitted June 2, 2008.

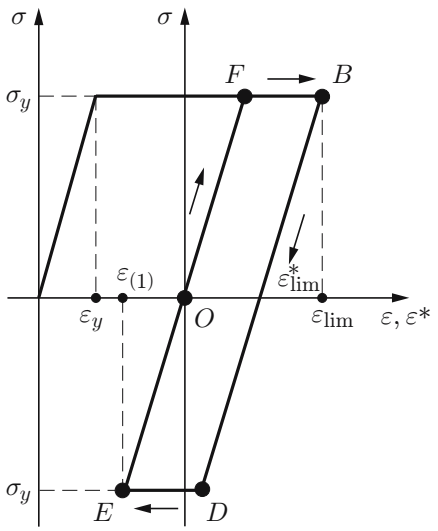

Fig. 1

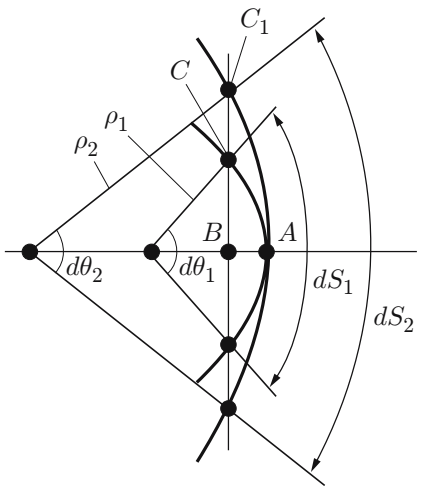

Fig. 2

Fig. 1. Diagram of tension of the sample under cyclic loading.

Fig. 2. Diagram of elastoplastic deformation of the crack tip in the first loading half-cycle.

the stress that would act the crack tip assuming that the sample material obeys Hook's law over the entire range of loads up to fracture.

Equality (1) is obtained for a prismatic rod with a hyperbolic concentrator made of any material which deforms nonlinearly and undergoes antiplane shear (K_{III} mode crack loading). In [1], it is assumed that this equality is also valid for other types of concentrators and loads. In [2], equality (1) was verified experimentally using the method of photoelastic coatings for axial tension of a rectangular strip with a circular hole made of D16T aluminum alloy. The results of these experiments confirmed the validity of formula (1). The same problem of extension of a rectangular strip of D16T alloy with a circular hole beyond the yield point was solved numerically [3]. The calculated stress and strain concentrations were substituted into the right side of Eq. (1) and compared with the concentration factor k_e for elastic extension [4]. The error was 5.3%. The aforesaid leads to the conclusion that formula (1) can be used to analyze the stress–strain state at the tips of crack-like defects, as is done, for example, in [5].

We write relation (1) using the notation adopted above. It should be noted that this equality is valid if, for zero stress, the strains are also equal to zero. However, for cyclic loading, the tensile diagram shows a hysteresis loop (Fig. 1). Therefore, we place the coordinate origin at the point O. In this coordinate system, the abscissa ε^* is related to the strain ε by the expression $\varepsilon^* = \varepsilon - (\varepsilon_{(1)} + \varepsilon_y)$. In the new coordinate system, the limiting strain is denoted by $\varepsilon^*_{\mathrm{lim}}$. As a result, we have the relation between the elastoplastic strain on the hole contour and the elastic stress that would act at the same point corresponding to the crack tip under the assumption of absolutely elastic deformation of the sample material:

$$\frac{\varepsilon^*}{\varepsilon_y} = \left(\frac{\sigma_e}{\sigma_y}\right)^2. \tag{2}$$

As a hypothesis we adopt the following.

Statement 1. *During loading, the points located on the crack faces move strictly in the direction of the external loading, i.e., perpendicular to the direction of the major half-axis of the elliptic crack.*

This statement is valid only if the crack is modeled by a mathematical cut (Westergaard's asymptotic elastic solution [6]). If the defect is a blunted crack, which can be approximately interpreted as a narrow elliptic hole in a sample having elastoplastic properties, this statement is not strictly valid. Considering the displacements of the point A at the crack tip and the point C located at the crack face infinitely close to the point A, we note the following circumstance: the horizontal displacements of these points are almost identical: $u_A \simeq u_C$, and the vertical

displacement v_C of the point C is a few orders of magnitude larger than the difference $u_A - u_C$. As evidence of this fact, we give the results of a finite-element calculations of elastoplastic deformation of a steel strip with an elliptic hole. The sample had the following sizes: height 100 cm, width 100 cm, length of the major axis of the ellipse 10 cm, and length of the minor axis 4 cm. The curvature radius is 8 mm. Under axial tension by a load perpendicular to the major half-axis of the ellipse, the displacements of the points A and C are $u_A = 98.71$ μm, $u_C = 98.46$ μm, $v_A = 0$, $v_C = 8.84$ μm, $u_A - u_C = 0.25$ μm, and $v_A - v_C = 8.84$ μm. In the present paper, we consider the shape change of the most dangerous region of the defect — its tip. If the final position of the crack tip is projected onto the initial position, it is obvious that, after loading, the point C is located, with accuracy to small quantities of higher orders, on a line perpendicular to the major half-axis of the ellipse.

At the tip of the unloaded crack, we distinguish an infinitesimal element dS_1 (Fig. 2) within which the deformation can be considered homogeneous throughout the loading cycle. Next, we increase the external load, resulting in crack opening — its faces begin to move apart. At the crack tip, an increase in strain is accompanied by an increase in the curvature radius, i.e., the crack becomes blunted. The point C located on the boundary of the element considered moves in the vertical direction to the point C_1. We fix the crack tip at this time. The length of the element is dS_2, and the curvature radius at the top $\rho = \rho_2$. Figure 2 shows the crack tip at the beginning and at the end of loading. The length of the segment AB is equal to

$$\rho_1(1 - \cos(d\theta_1/2)) = \rho_2(1 - \cos(d\theta_2/2)).$$

Expanding the cone in a power series and ignoring small quantities of higher orders ($d\theta \ll 1$), we obtain

$$\rho_1\, d\theta_1^2 \simeq \rho_2\, d\theta_2^2. \tag{3}$$

The lengths of the arcs are expressed as follows: $dS_1 = \rho_1\, d\theta_1$ and $dS_2 = \rho_2\, d\theta_2 = dS_1 + \Delta\, dS_1 = dS_1(1 + \varepsilon)$. Here $\varepsilon = \Delta\, dS_1/dS_1$ is the strain of the element during crack opening. Taking into account (3), at the end of the loading, the curvature radius at the crack tip is equal to

$$\rho_2 = \rho_1(1 + \varepsilon)^2. \tag{4}$$

3. First Loading Cycle. The external stresses increase from the value $\sigma_{\min}$ to the value $\sigma_{\max}$. In the beginning of the first half-cycle, the stress–strain state of the point at the crack tip is described by the point E in the tension diagram (see Fig. 1). This point corresponds to the stress $-\sigma_y$, strain $\varepsilon_{(1)}$, curvature radius at the tip ρ_1, defect length $2l$, and external stress $\sigma_{\min}$. As the external load is increased, two opposed processes develop simultaneously: an increase in the elastoplastic strain at the crack tip and an increase in the curvature radius at the crack tip, resulting in a decrease in the strain concentration factor and, hence, elastoplastic strain. The crack geometry (curvature radius) is adjusted to the load level so that, during the growth in the external stress, the maximum strain at the crack tip did not exceed the limiting level. If this condition is satisfied at the end of the first half-loading cycle, the crack does not increase.

However, if the strain at the crack tip reaches the limiting level before the external loading has reached the value $\sigma_{\max}$, a further increase in the curvature radius at the crack tip will be possible only by fracture of the sample material. Taking into account that the load at the crack tip is considered rigid, and examining the displacement of the point C (see Fig. 2), we distinguish the following stages of the process.

1. Let, at a certain value of the external stress ($\sigma < \sigma_{\max}$), the point C coincides with the point C_1. In this case, the strain in an infinitesimal element is equal to the limiting value $\varepsilon^*_{\lim}$. The material at the crack tip does not fracture.

2. The external load increases by a small quantity $\Delta\sigma$. As a result, the point C travels a small distance to the point C_1' (Fig. 3a). In this case, the strain at the crack tip exceeds the limiting value, resulting in fracture of the material at the crack tip (in Fig. 3a, this part of the sample is hatched). We assume that the material loosened, i.e., disappeared. As a result, the crack tip moves forward and the curvature radius at the crack tip increases, leading to a reduction in the strain concentration. Hence, at the points of the crack tip formed, the strain does not exceed the limiting value.

3. Upon a further increase in the external load by a quantity $\Delta\sigma$, the point C moves to the point C_1'' (Fig. 3b). The strain at the crack tip again exceeds the limiting level, resulting in further fracture of the sample material (the hatched region in Fig. 3b). This, in turn, leads to an increase in the crack length and curvature radius and to a decrease in the crack-tip strain to the value $\varepsilon^*_{\lim}$.

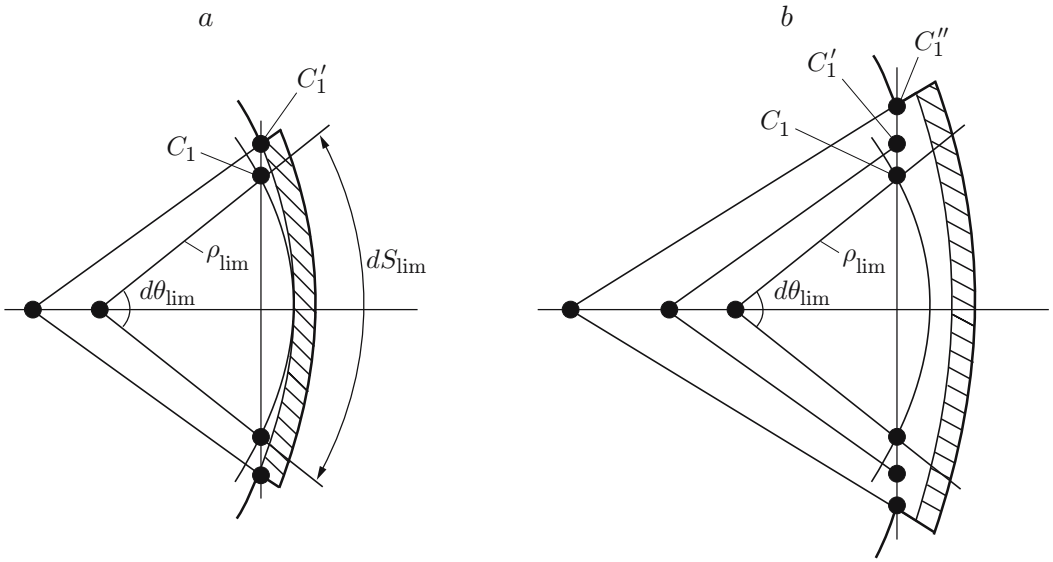

Fig. 3. Diagram of crack growth in the elementary acts of additional loading: (a) the first act of additional loading; (b) the second act of additional loading; the hatched regions are the regions of fracture of the sample.

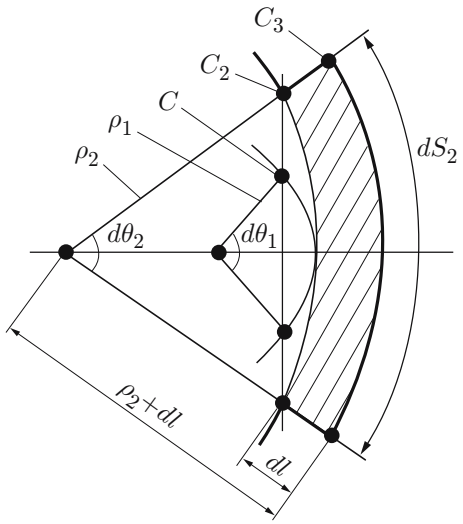

Fig. 4. Diagram of crack growth in the first half-loading cycle: the hatched region is the region of fracture of the sample.

4. The process continues until the external stress reaches the value $\sigma_{\max}$, and the point C moves to the point C_2 (Fig. 4). In this case, as a result of numerous fractures in the elementary acts of additional loading, the crack half-length increases by a quantity dl. The curvature radius at the crack tip increases by the same quantity.

If the sample material operates beyond the yield point, the superposition principle is usually inapplicable. In this case, however, its use is justified. Since the loading of the crack is rigid, the geometry of the crack tip does not change at the end of the first half-loading cycle (position of the point C_3) regardless of how the fracture proceeded: by sequential rupture of the fibers located at the crack tip or by fracture of part of the material of width dl after the point C has moved to the point C_2 (see Fig. 4). In view of this circumstance, we first determine the strain $\varepsilon^*_{\max}$ that arises in the region adjoining the crack tip when the sample is loaded by external stress from the value $\sigma_{\min}$

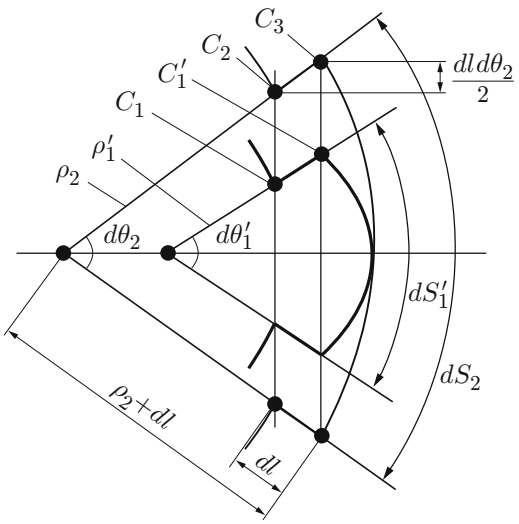

Fig. 5. Diagram of elastoplastic deformation of the crack tip in the second loading half-cycle.

to the value $\sigma_{\max}$ under the assumption that the material does not fracture. The elastic stress at the crack tip is written as

$$\sigma_e = k_e(\sigma_{\max} - \sigma_{\min}) - \sigma_y \simeq 2\sqrt{l/\rho_1}\,\sigma_{\max}(1-r) - \sigma_y.$$

Here the concentration factor k_e [7] is written taking into account that $l \gg \rho_1$ and $r = \sigma_{\min}/\sigma_{\max}$ is the asymmetry coefficient of the loading cycle. Then, in view of equality (2), the strain increment in the half-loading cycle from the value $\sigma_{\min}$ to the value $\sigma_{\max}$ can be represented as

$$\varepsilon^*_{\max} = \varepsilon_y\Big(2\sqrt{\frac{l}{\rho_2}}\,\frac{\sigma_{\max}(1-r)}{\sigma_y} - 1\Big)^2.$$

From this, taking into account (4), we obtain

$$\varepsilon^*_{\max} = \Big(\frac{\sqrt{\varepsilon_{ep}}}{1+\varepsilon^*_{\max}} - \sqrt{\varepsilon_y}\Big)^2, \tag{5}$$

where ε_{ep} is the elastoplastic strain that would arise at the crack tip under loading from the stress $\sigma_{\min}$ to $\sigma_{\max}$ under the assumption that the curvature radius of the crack does not change:

$$\varepsilon_{ep} = \varepsilon_y\Big(2\sqrt{\frac{l}{\rho_1}}\,\frac{\sigma_{\max}(1-r)}{\sigma_y}\Big)^2. \tag{6}$$

If $\varepsilon^*_{\max} \leqslant \varepsilon^*_{\lim}$, the crack does not increase. Otherwise, fracture (loosening) of part of the material at the crack tip occurs (hatched region in Fig. 4), resulting in an increase in the curvature radius to the value $\rho_2 + dl = \rho_1(1+\varepsilon^*_{\max})^2 + dl$ [see (4)] and an increase in the strain to the limiting value $\varepsilon^*_{\lim}$. In view of this, we write equality (2) as

$$\varepsilon^*_{\lim} = \varepsilon_y\Big(2\sqrt{\frac{l+dl}{\rho_2+dl}}\,\frac{\sigma_{\max}(1-r)}{\sigma_y} - 1\Big)^2.$$

From this, after some transformations taking into account that $dl \ll l$, we obtain the following increment in the crack half-length at the end of the first loading half-cycle:

$$dl = \rho_1\Big(\frac{\varepsilon_{ep}}{(\sqrt{\varepsilon^*_{\lim}} + \sqrt{\varepsilon_y})^2} - (1+\varepsilon^*_{\max})^2\Big)dN. \tag{7}$$

Here it is taken into account that the increment dl occurred for the minimum possible number of loading cycles $dN = 1$.

4. Second Loading Half-Cycle. As the external stress decreases from the value $\sigma_{\max}$ to the value $\sigma_{\min}$, the crack tip configuration is restored to the initial one that was at the beginning of the loading cycle: the curvature radius at the tip should decrease to a value close to the value ρ_1. However, since the strain of the region adjoining the crack tip is rigid, the length of the segment C_3C_1' (Fig. 5) traveled by the point C_3 in the second half-loading cycle should be equal to the length of the segment CC_2 traveled by the point C in the first half-cycle (see Fig. 4). As above, is its assumed that, during loading, the crack faces move along lines perpendicular to the major half-axis of the defect. At the end of the second loading half-cycle (see Fig. 5), the arc length is equal to $dS_1' = \rho_1'\, d\theta_1' = \rho_1\, d\theta_1 + dl\, d\theta_2$. In view of this, ignoring small quantities of higher orders, we obtain the curvature radius at the crack tip at the end of the loading cycle:

$$\rho_1' = \rho_1 + \frac{2\,dl}{1+\varepsilon_{\max}^*} = \rho_1\Big(1 + \frac{2\,dl}{\rho_1(1+\varepsilon_{\max}^*)}\Big). \tag{8}$$

Thus, in the full loading cycle, the curvature radius increases. In this case, the additive $2\,dl/[\rho_1(1+\varepsilon_{\max}^*)]$ can be small compared to unity. However, in the case of multicycle fatigue resulting from repeated loading, this additive can lead to a significant change in the curvature radius at the crack tip.

During the second half-loading cycle, the material at the crack tip is subjected to the compressive strain ε_c^*. We write relation (4) as $\rho_2 + dl = \rho_1'(1+\varepsilon_c^*)^2$. In view of (8), the obtained equality becomes

$$\varepsilon_c^* = \sqrt{\frac{\rho_1(1+\varepsilon_{\max}^*)^2 + dl}{\rho_1 + 2\,dl/(1+\varepsilon_{\max}^*)}} - 1.$$

The same strain can be obtained from condition (2):

$$\varepsilon_c^* = \varepsilon_y\Big(2\sqrt{\frac{l}{\rho_1'}}\,\frac{\sigma_{\max}(1-r)}{\sigma_y} - 1\Big)^2.$$

In view of relations (6) and (8), this expression becomes

$$\varepsilon_c^* = \Big(\sqrt{\frac{\varepsilon_{ep}}{1+2\,dl/[\rho_1(1+\varepsilon_{\max}^*)]}} - \sqrt{\varepsilon_y}\Big)^2.$$

As a result, in view of equality (7), we obtain the system of nonlinear equations

$$\begin{gathered}\sqrt{\frac{\rho_1(1+\varepsilon_{\max}^*)^2 + dl}{\rho_1 + 2\,dl/(1+\varepsilon_{\max}^*)}} - 1 = \Big(\sqrt{\frac{\varepsilon_{ep}}{1+2\,dl/[\rho_1(1+\varepsilon_{\max}^*)]}} - \sqrt{\varepsilon_y}\Big)^2,\\ \frac{dl}{dN} = \rho_1\Big(\frac{\varepsilon_{ep}}{(\sqrt{\varepsilon_{\lim}^*} + \sqrt{\varepsilon_y})^2} - (1+\varepsilon_{\max}^*)^2\Big),\end{gathered} \tag{9}$$

whose solution yields the limiting strain $\varepsilon_{\lim}^*$ and fatigue crack growth rate. At $2\,dl/[\rho_1(1+\varepsilon_{\max}^*)] \ll 1$, the problem is considerably simplified. In this case, the solution of system (9) can be obtained in explicit form

$$\tilde{\varepsilon}_{\lim} \simeq \Big(\frac{\sqrt{\varepsilon_{ep}}}{1+(\sqrt{\varepsilon_{ep}} - \sqrt{\varepsilon_y})^2} - \sqrt{\varepsilon_y}\Big)^2;$$

$$\frac{dl}{dN} \simeq \rho_1\Big[\Big(1 + \Big(\sqrt{\varepsilon_{ep}} - \sqrt{\varepsilon_y}\Big)^2\Big)^2 - (1+\varepsilon_{\max}^*)^2\Big]. \tag{10}$$

Further simplification is possible provided that $\sqrt{\varepsilon_{ep}} \gg \sqrt{\varepsilon_y}$. In this case, equality (10) reduces to the relation

$$\frac{dl}{dN} \simeq \rho_1[(1+\varepsilon_{ep})^2 - (1+\varepsilon_{\max}^*)^2]. \tag{11}$$

If $\varepsilon_{\max}^* \ll 1$, Eq. (5) can be linearized to yield $\varepsilon_{\max}^* \approx \varepsilon_{ep}/(1+2\varepsilon_{ep})$. Then, the expression for the fatigue crack growth rate can be rearranged to give

$$\frac{dl}{dN} \approx \rho_1\varepsilon_{ep}^2. \tag{12}$$

It should be noted that, in view of relation (5), the final formulas for the fatigue crack growth rate (10)–(12) are expressed in terms of one parameter ε_{ep}, which, in turn, can be expressed in terms of the stress intensity factor commonly used in fracture mechanics [8]. In the case of cyclic loading, we have

$$K_{\mathrm{I}\max} = \sigma_{\max}\sqrt{\pi l}, \qquad K_{\mathrm{I}\min} = \sigma_{\min}\sqrt{\pi l}.$$

Here $K_{\mathrm{I}\max}$ and $K_{\mathrm{I}\min}$ are the stress intensity factors calculated for the maximum and minimum stresses of the loading cycle. Denoting the amplitude of the stress intensity factor by $\Delta K = K_{\mathrm{I}\max} - K_{\mathrm{I}\min}$, we express the strain ε_{ep} [see (6)] as

$$\varepsilon_{ep} = \frac{4}{\pi\rho_1 E\sigma_y}\,\Delta K^2.$$

Thus, the analysis of equalities (10)–(12) leads to the conclusion that the fatigue crack growth rate is proportional to the quantity ΔK^4. For example, equality (12) becomes

$$\frac{dl}{dN} \approx \frac{16}{\pi^2\rho_1 E^2\sigma_y^2}\,\Delta K^4. \tag{13}$$

We note that formula (13) is similar in structure to the Paris empirical relation [8]

$$\frac{dl}{dN} = C(\Delta K)^4.$$

Thus, the model considered here allows steady-state fatigue crack growth to be explained in terms of the classical mechanics of continuous homogeneous continuum. According to the proposed concept, the main factor responsible for the development of fatigue damage is a change in the elastoplastic strain concentration at the crack tip during cyclic loading of the sample. In the first half-loading cycle, there is an increase in the elastoplastic strain, resulting in an increase in the curvature radius at the crack tip. The crack does not grow until the strain is lower than the limiting value for the given material. With a further increase in the external load, if the crack-tip strain exceeds the limiting level, an increase in the curvature radius (and, hence, a reduction in the strain concentration factor) will be possible only by fracture of part of the sample material directly ahead of the crack tip, resulting in crack growth. As a consequence, the resulting geometry of the crack tip provides the limiting elastoplastic strains. In the second half-loading cycle, the crack tip geometry and the size of the plastic zone are partly restored to the initial state that was at the beginning of the loading cycle.

The author thanks M. Kh. Akhmetzyanova for useful discussions of the work.

REFERENCES

1. H. R. Neuber, "Theory of stress concentration for shear-strained prismatic bodies with arbitrary nonlinear stress–strain law," *Mekhanika*, No. 4, 117–130 (1961).
2. A. Ya. Aleksandrov and M. Kh. Akhmetzyanov, *Polarization Optical Methods of Mechanics of Deformable Solids* [in Russian], Nauka, Moscow (1973).
3. O. E. Klochko and A. P. Shabanov, "Using a finite element method to calculate stress concentration at the tips of defects of small radius," *Vest. SGUPS*, No. 12, Siberian State University of Means of Communication, Novosibirsk (2005), pp. 47–51.
4. R. E. Peterson, *Stress Concentration Factors*, Wiley, New York (1974).
5. V. F. Luk'yanov and V. N. Fomin, "Engineering method for calculating the fracture toughness parameter," *Probl. Prochnosti*, No. 2, 55–59 (1972).
6. V. M. Pestrikov and E. M. Morozov, *Fracture Mechanics of Solids* [in Russian], Professiya, St. Petersburg (2002).
7. H. Neuber, *Kerbspannunglehre: Grunglagen für Genaue Spannungsrechnung*, Springer-Verlag (1937).
8. G. R. Irwin and P. C. Paris, "Fundamental aspects of crack growth and fracture," in: H. Liebowitz (ed.), *Fracture. An Advanced Treatise*, Vol. 3: *Engineering Fundamentals and Environmental Effects*, Academic Press, New York–London (1971).